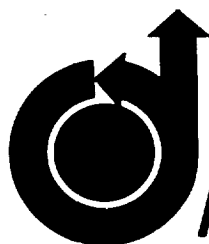


NASA/TM- 81- 207525

NIS

711-34-TM

074654



AIAA-81-0333

**A Reattaching Free Shear Layer
in Compressible Turbulent
Flow—A Comparison of
Numerical and Experimental Results**

C.C. Horstman, NASA Ames
Research Center, Moffett Field,
Ca.; and G.S. Settles, S.M.
Bogdonoff and D.R. Williams,
Princeton University, Princeton, N.J.

**AIAA 19th
AEROSPACE SCIENCES MEETING**

January 12-15, 1981/St. Louis, Missouri

A REATTACHING FREE SHEAR LAYER IN COMPRESSIBLE TURBULENT FLOW —
A COMPARISON OF NUMERICAL AND EXPERIMENTAL RESULTS

C. C. Horstman*
Ames Research Center, NASA
Moffett Field, California

and

G. S. Settles,[†] D. R. Williams,[‡] and S. M. Bogdonoff[§]
Princeton University
Princeton, N. J.

Abstract

An investigation of a two-dimensional, free turbulent shear layer reattaching on an inclined surface at Mach 2.92 and at a high Reynolds number is described. The test geometry is specifically designed to isolate the reattachment process of a high-speed separated flow. A numerical solution of the time-dependent, Reynolds-averaged, Navier-Stokes equations for the entire flow field, employing a two-equation eddy viscosity turbulence model, is presented. Detailed comparisons of prediction and experiment are made in the free shear layer, at reattachment, and in the developing boundary layer downstream. These comparisons include mean surface quantities as well as mean and fluctuating flow-field quantities. Although the overall features of this complex flow field are predicted, there are several deficiencies in the numerical solution, particularly in the region downstream of reattachment. Modifications of the turbulence model to correct these deficiencies are discussed.

x' = distance along ramp measured from leading edge (Fig. 1)
 y = distance normal to model surface: measured from plane of upstream flat plate in free shear layer; measured from model surface on ramp
 γ^* = exponential damping term in turbulence model
 δ = shear-layer or boundary-layer thickness
 δ^* = boundary-layer displacement thickness
 θ = boundary-layer momentum thickness
 μ = molecular viscosity
 μ_t = turbulent eddy viscosity
 ρ = density
 τ = shear stress
 ω = turbulent dissipation rate

Nomenclature

C_{f_∞} = skin friction coefficient based on free-stream conditions
 k = turbulent kinetic energy, $(\overline{u'^2} + \overline{v'^2} + \overline{w'^2})/2$
 l = turbulent length scale, \sqrt{k}/ω
 M = Mach number
 p = static pressure
 R_t = turbulence Reynolds number
 u = velocity in x or x' direction
 v = velocity in y direction
 w = velocity normal to u and v
 x = streamwise distance measured from separation corner (Fig. 1)

Subscripts

max = maximum
 w = wall conditions
 ∞ = free-stream conditions

Superscripts

$()'$ = fluctuating quantity
 $\langle () \rangle$ = rms value

Introduction

In the past several years, considerable advances have been made in the prediction of compressible viscous flow fields. For two-dimensional flows, with both adverse and favorable pressure gradients and even with small separated regions, various computational methods employing a two-equation eddy viscosity turbulence model do an adequate job of predicting the flow fields.^{1,2} However, the computation of flow fields in which there are large separated zones has only met with limited success.²⁻⁴ Large disagreements between numerical and experimental results are most prevalent in the reattachment region and downstream. Unfortunately, in these latter viscous compressible flow interactions, boundary-layer separation and subsequent reattachment are often intimately connected and it

*Assistant Chief, Experimental Fluid Dynamics Branch, Associate Fellow AIAA.

[†]Professional Research Staff Member and Lecturer, Mechanical and Aerospace Engineering, Member AIAA.

[‡]Graduate Research Assistant.

[§]Professor and Chairman, Mechanical and Aerospace Engineering, Fellow AIAA.

This paper is declared a work of the U.S. Government and therefore is in the public domain.

is difficult to scrutinize either phenomenon by itself.

A recent experimental investigation performed at Princeton University⁵ has successfully isolated the reattachment process of a high-speed separated flow. This offers a unique opportunity to test the ability of a numerical technique and its associated turbulence model to correctly model the reattachment region and downstream boundary-layer redevelopment without the additional complication of modeling the separation process as well. In this study, an equilibrium turbulent boundary layer developed on a flat plate. The layer then separated at a sharp corner, forming a free shear layer that bridged a cavity to reattach upon an inclined ramp. The measurements included detailed mean surface and flow-field data as well as mass-flow fluctuation data in the flow field.

This paper presents a detailed comparison of numerical calculations and experimental results for the reattaching free shear layer described above. The calculations employed are solutions of the time-dependent, Reynolds-averaged, Navier-Stokes equations, using a two-equation eddy viscosity turbulence model.¹ These comparisons test the ability to calculate not only the reattachment process and downstream boundary-layer growth, but also the development of the supersonic free shear layer. These three problems are, in a sense, separate and provide a severe test of the turbulence model and the computational techniques used. Based on these comparisons, deficiencies in the turbulence model are discussed and modifications to correct these deficiencies are proposed.

Description of Experiment

The experiment was conducted in the Princeton University 20 x 20-cm High Reynolds Number Supersonic Wind Tunnel at a free-stream Mach number of 2.92 and a unit Reynolds number of $6.7 \times 10^7/\text{m}$ (Ref. 5). A sketch of the test model is shown in Fig. 1. A turbulent boundary layer developed initially on the flat plate (22.9 cm long), then separated over the sharp backward-facing step. The resulting free shear layer bridged a 2.54-cm-deep cavity and reattached on a plane ramp inclined 20° to the horizontal. The movable ramp was adjusted so

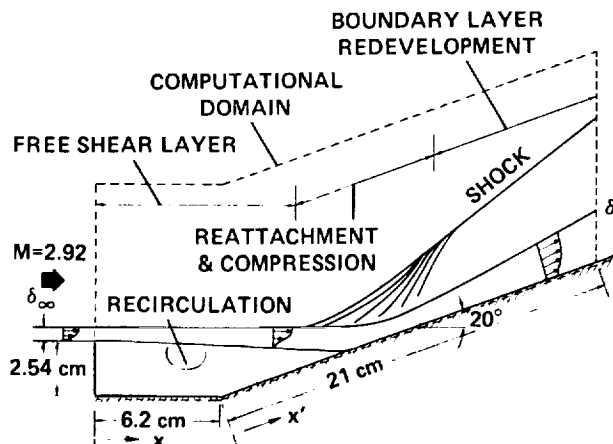


Fig. 1 Flow geometry and computational domain.

that there was essentially no change in pressure or flow direction when the boundary layer separated. (The average value of the ratio of plate pressure to cavity pressure over the test series was 1.04.) Two-dimensionality was verified with surface streak patterns and spanwise surface pressure and Preston tube measurements.

The measurements included surface pressure and skin friction, mean flow-field pressure and velocity distributions, and mass-flow fluctuations throughout the flow field. The skin friction data were obtained with Preston tubes and verified by combined wall-wake-law velocity-profile correlations. The mean velocity data were obtained from pitot and static pressure and total temperature measurements. Hot-wire anemometers were used to obtain the mass-flow fluctuations. Further details of the experimental techniques and results are contained in Ref. 5.

Solutions to the Navier-Stokes Equations

The partial differential equations used to describe the mean flow field are the time-dependent, Reynolds-averaged Navier-Stokes equations for two-dimensional flow of a compressible fluid. Restrictions on the equations include the perfect gas assumption, constant specific heats, the Sutherland viscosity law, and zero bulk viscosity. The Wilcox-Rubesin¹ two-equation model was chosen for turbulence closure. The use of an algebraic eddy-viscosity turbulence model did not seem feasible for this complex flow field. The problem is the a priori specification of a length scale everywhere in the flow field. This would be especially difficult in the large recirculation zone and in the reattachment region where the length scale must make the transition from a free shear layer to an attached boundary layer. As a first effort to solve this flow field, the use of the two-equation model, which calculates its own length scale, seemed appropriate.

For the Wilcox-Rubesin two-equation model, the flow-field equations are augmented by two additional partial differential equations: one for the turbulent kinetic energy k and another for the square of the dissipation rate ω^2 . The Wilcox-Rubesin model uses the eddy-viscosity hypothesis; that is, the Reynolds stress, turbulent heat-flux, and kinetic-energy flux terms are assumed to be related to the mean-flow velocity, temperature, and kinetic energy gradients through an eddy transport coefficient that is simply added to the corresponding molecular viscosity or transport coefficient. The turbulent eddy viscosity μ_t is expressed in terms of k and ω :

$$\mu_t = \gamma^* \rho \frac{k}{\omega}$$

where γ^* is an exponential damping term that depends on a turbulent Reynolds number, $R_t = \rho \sqrt{k} \ell / \mu$. This Reynolds number is based on a length scale of the turbulence, ℓ , defined as $\ell = \sqrt{k} / \omega$. The complete equations, including the equations and constants for the turbulence model, are described in Ref. 2.

Numerical Method

The numerical procedure used here is the basic explicit second-order, predictor-corrector,

finite-difference, time-splitting method of MacCormack,⁶ modified by the efficient explicit-implicit-characteristic algorithm of Ref. 7. A description of this method, along with its adaptation to multiequation turbulence models, is contained in Refs. 2 and 8.

Computational Domain

The computational domain is shown in Fig. 1. The upstream boundary was placed at the separation corner to avoid possible difficulties there. A mesh was developed that allowed a variable point spacing in each coordinate direction. One set of grid lines was placed normal to the free-stream direction and the other parallel to the model surface. The total mesh size was 90 points in the streamwise direction and 82 points normal to the model surface. In the streamwise direction mesh spacing varied from 0.065 cm near the corner to 0.50 cm near the downstream boundary. In the direction normal to the surface an exponentially stretched spacing was used near the wall followed by a uniform spacing. The distance of the first y mesh point from the model wall was selected small enough so that the solutions are independent of spacing (typically within $y^+_{\min} \equiv y\sqrt{\tau_w \rho_w / \mu_w} < 0.5$).

Boundary Conditions

The boundaries of the computational mesh extended in the vertical direction from the model surface to the free stream and in the flow direction from $x = 0$ to $x' = 21$ cm. The upstream boundary conditions were prescribed by a combination of uniform free-stream conditions and the result of a boundary-layer computation¹ along the flat-plate surface. The boundary-layer program was run for a distance that insured a match of the experimental and numerical boundary-layer displacement thicknesses at $x = -2.54$ cm. At the vertical wall below the corner, the pressure was set equal to the free-stream pressure (to match the experimental results), and the temperature was set equal to the model wall temperature. The vertical velocity was set equal to zero and the horizontal velocity was set equal to $0.0005 u_\infty$. (When an inflow velocity of zero was used a solution could not be obtained.) The downstream boundary was positioned far enough aft so that all of the gradients in the flow direction could be set to zero. This boundary condition was verified by the lack of any substantial change in the numerical results when the location of the downstream boundary was changed. At the model surface, no-slip boundary conditions are applied along with a constant wall temperature. Additional details concerning the boundary conditions for the turbulence model near the model surface are discussed in Ref. 2. The upper boundary is specified by the free-stream conditions. The free-stream disturbance level was set at $\sqrt{k}/u_\infty = 0.006$, which amounts to $\langle(\rho u)'\rangle/\rho_\infty u_\infty = 0.025$.

Results and Discussion

A map of the computed Mach contour lines in the flow field is shown in Fig. 2. In agreement with the experimental results, the incoming turbulent boundary layer separates at the corner without turning, forming a free shear layer. This layer spreads more rapidly into the cavity than into the outer, supersonic flow, and reattaches on the ramp at a point slightly below the geometric extension of the flat plate onto the ramp surface. The average

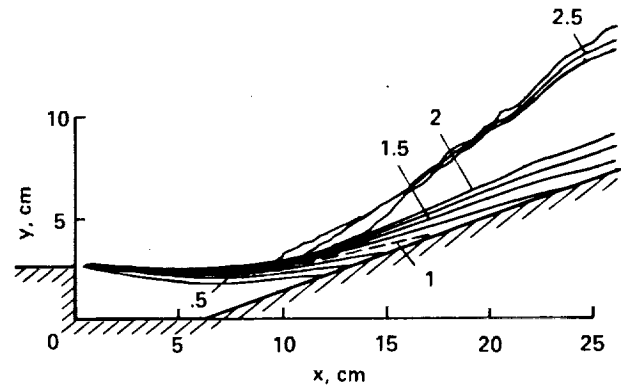


Fig. 2 Computed contour plot of Mach number.

computed pressure on the cavity floor was $0.97 p_\infty$, which agrees exactly with the experiment. Downstream of reattachment a new boundary layer develops on the ramp. Detailed comparisons with the experimental data are presented in two parts: the free-shear-layer results and the reattachment and downstream boundary-layer results.

Free Shear Layer

The computed and experimental velocity profiles are compared at several streamwise locations in the free shear layer in Fig. 3. Also shown is a comparison of computed and experimental boundary-layer profiles upstream of the separation point on the flat plate ($x = -2.54$ cm). These upstream results were computed using the boundary-layer code mentioned earlier. In the shear layer the computed results are in good agreement with the experiment for velocity ratios greater than 0.5. However, for the lower velocity ratios the computed results are substantially greater than the data. This indicated that the computed shear layer spread into the cavity farther than the measured one, resulting in a larger shear-layer thickness before reattachment. At the lower values of velocity the viscous terms in the momentum equation become relatively more important, so any lack of validity in the turbulence model equations is expected to cause larger differences

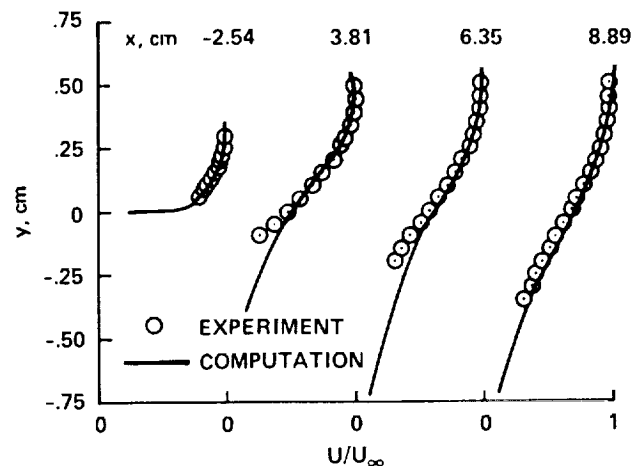


Fig. 3 Comparison of computations and velocity profile measurements in the free shear layer.

between the computations and measurements in this region. Apparently the turbulence model produces too much diffusion here. At the last station compared ($x = 8.89$ cm), the results show better agreement than for the previous stations. The maximum computed reverse velocity in the cavity is $0.17 u_\infty$; however, experimental data were not obtained in this region, and no comparison is possible.

The free-shear-layer spreading rates for both the experimental and the computed results have been calculated by defining the shear-layer thickness, δ , as the distance between $(u/u_\infty)^2 = 0.1$ and 0.9 (ref. 9). The spreading rate was evaluated after velocity profile similarity developed in the shear layer, which required a distance downstream of separation of 18 initial boundary-layer thicknesses in the experiment and 22 thicknesses in the computation. A comparison is shown in Fig. 4 along with a line representing average values from previous high-Reynolds-number, compressible, free-shear-layer experiments.¹⁰ Although the computed profile shapes were not in good agreement with experiment, the growth rate of the width of the profile is in good agreement.

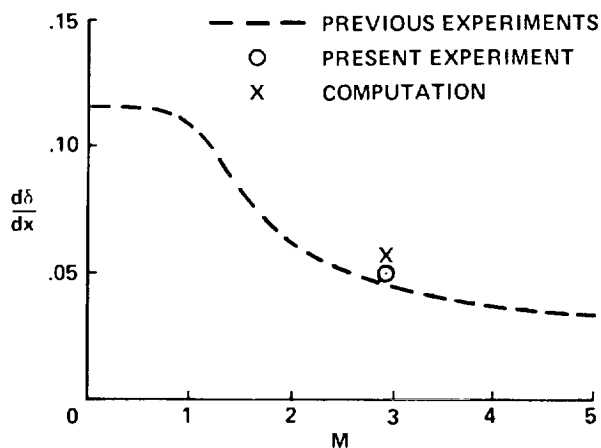


Fig. 4 Comparison of computation and free-shear-layer spreading rate measurements.

The present computations provide a significant improvement over previous computational results,¹⁰ which predicted the incompressible value of the spreading rate ($d\delta/dx = 0.12$) at supersonic Mach numbers. More recent computations by Saffman¹¹ and by Oh and Bushnell¹² also predict the correct compressible spreading rates. Saffman's turbulence model is an earlier version of the one used in the present computations; in the model used by Oh and Bushnell an additional term modeled the pressure-velocity correlation, which was a function of Mach number. The present calculations require no additional terms for compressible flow. It is significant that the present computational framework has captured the physics of this compressible spreading phenomenon, even though the phenomenon is known to violate Morkovin's hypothesis.¹³

The computed and experimental rms mass-flow fluctuations are compared at several streamwise locations in the free shear layer in Fig. 5. Also shown is a comparison upstream of the separation point on the flat plate ($x = -0.76$ cm). To compare the computed and measured turbulent fluctuations several assumptions were made. The mass-flow

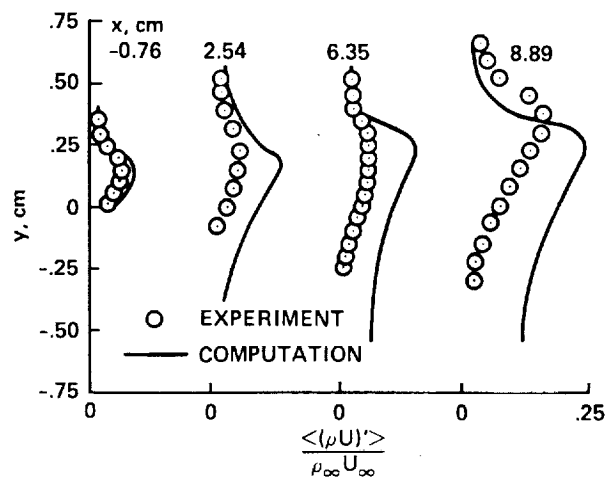


Fig. 5 Comparison of computations and rms mass-flow fluctuation profile measurements in the free shear layer.

fluctuations were measured experimentally, and the total turbulent kinetic energy was computed and converted to rms mass-flow fluctuations, $\langle \rho u \rangle'$. This latter computation was carried out as follows. It was assumed that the ratio of the streamwise to lateral to normal velocity fluctuations was 4:3:2, and that the total temperature and pressure fluctuations were negligible compared with the streamwise velocity fluctuations. Thus the mass-flow fluctuations become a function of the computed turbulent kinetic energy, local Mach number, and density.¹⁴ For adiabatic flows away from shock waves these assumptions are reasonable¹⁴ and should provide at least a qualitative comparison of the experimental and computed results. But the validity of these assumptions is unknown within the shock-boundary-layer interaction.

In general the measured mass-flow fluctuation values are overpredicted throughout the flow field. In the lower part of the shear layer the data are overpredicted by a factor of 10. This large overprediction in the cavity is the result of too much diffusion in the turbulence-model equations at low velocities, which leads to incorrect mean velocity profiles, as shown in Fig. 3. At the last station ($x = 8.89$ cm) the computed and experimental results are at least qualitatively similar, though the levels disagree.

To examine the rate of growth of the fluctuation levels, both the measured and computed peak values have been normalized by their upstream values and plotted in Fig. 6. This comparison shows that the measured normalized peak values do not increase in magnitude until far downstream where velocity profile similarity is reached ($x \sim 6$ cm). The computed normalized peak values increase gradually until similarity is reached ($x \sim 7$ cm) and then increase more rapidly downstream. The agreement between the computed and measured values at the downstream location could be fortuitous.

Since the mass-flow fluctuations were grossly overpredicted in the lower part of the shear layer, it may be instructive to examine the computed turbulent length-scale distribution through the shear layer. The computed values of the mean velocity ratio and of the turbulent length scale, normalized

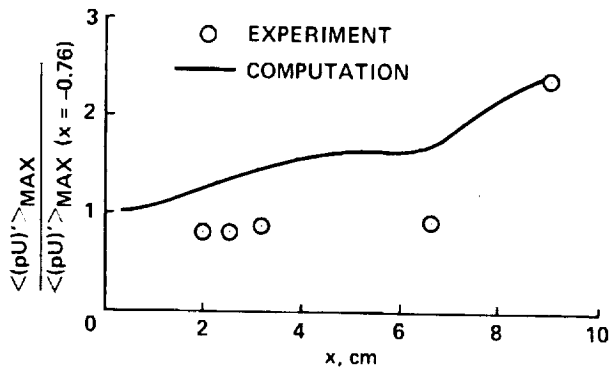


Fig. 6 Comparison of computations and maximum rms mass-flow fluctuation measurements in the free shear layer.

by the shear-layer thickness, are shown in Fig. 7 for $x = 6.35$ cm. The results show that the length scale increases continuously as y and the velocity ratio decrease. It is believed that this behavior is incorrect, and that the length scale should reach a maximum in the shear layer and then decrease as y decreases. However, there are no measurements available to support this speculation. If so, then any turbulence model improvements should be directed toward the length scale or the dissipation equation.

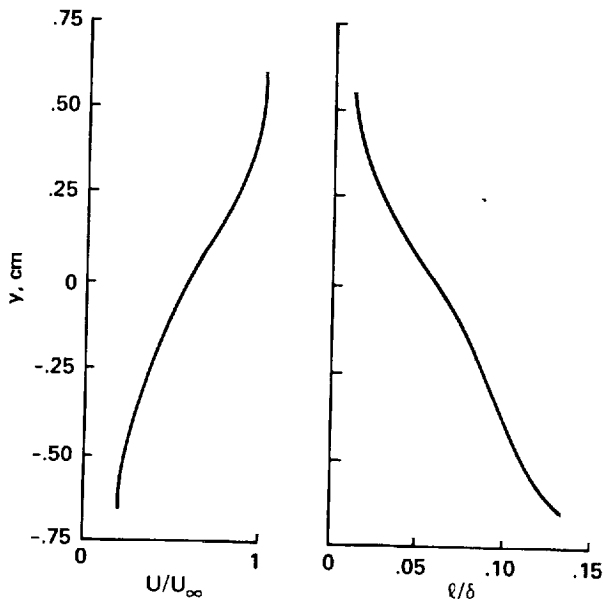


Fig. 7 Computed velocity and length scale profile in the free shear layer, $x = 6.35$ cm.

Reattachment and Boundary-Layer Redevelopment

Comparisons of the computed and experimental surface pressure and skin-friction distributions on the ramp are shown in Fig. 8. There is general qualitative agreement between the computed and measured values but several important differences are also noted. First, the computed reattachment point is at 5.2 cm, and the experimental reattachment point is at 6.76 cm. This difference is a result of the computed shear layer extending too far into the cavity, thus reattaching to the ramp surface too far upstream. This also explains the differences between

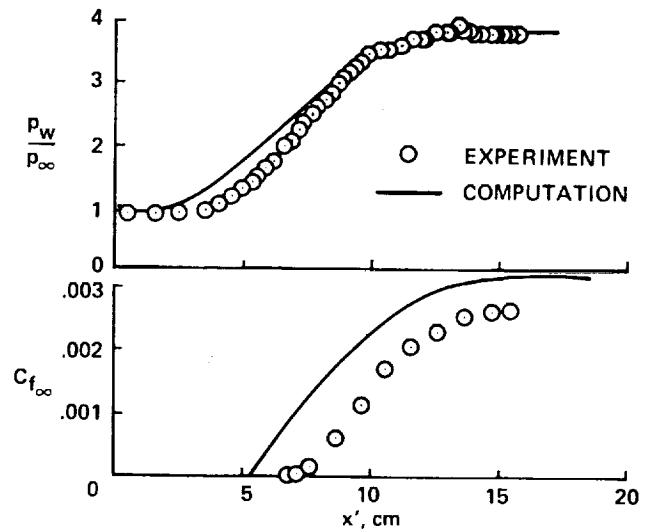


Fig. 8 Comparison of computations and measured surface pressure and skin friction on the reattachment ramp.

the predicted and measured pressure distributions. The predicted pressure first increases upstream of the experimental pressure increase, and requires about a 12% greater distance to reach its final value. Since the computed shear-layer thickness was also about 12% larger than the experimental value, these results are reasonable and in agreement with the free interaction theory discussed in Ref. 5. At the downstream end of the interaction the pressure is correctly predicted, but the skin friction is overpredicted by 20%.

Figure 9 compares the computed and experimental development of the boundary-layer thickness, displacement thickness, and momentum thickness downstream of reattachment. Although the correct trends of all three thicknesses are predicted, the values are too large. The boundary-layer thickness is overpredicted by as much as 60%. This is because the incoming shear layer is thicker than the experimental shear layer and because the large overprediction of turbulent kinetic energy and length scale in the lower portion of the incoming shear layer also tends to thicken the boundary-layer at reattachment. To allow a comparison of computed and experimental flow development downstream of reattachment despite this difference in thickness, the distances from the wall have been normalized by the local boundary-layer thickness in the remaining figures.

The computed and experimental static pressure profiles are compared at several streamwise locations in Fig. 10. The first station is located at the experimental reattachment point. In the boundary layer ($y/\delta < 1$), the predicted distributions show a larger variation normal to the surface than do the measured values. However, if the pressure increase due to turbulent kinetic energy ($2/3\rho k$) were added to the computed static pressure, the agreement with the experiment would improve. This correction is up to 15% for the present flow field. This was not done because the experimental results were obtained with a static pressure probe that is probably insensitive to this increased kinetic pressure. In the outer portion of the flow the calculated results show the correct trends, and differences between the computation and the experiment can be attributed to

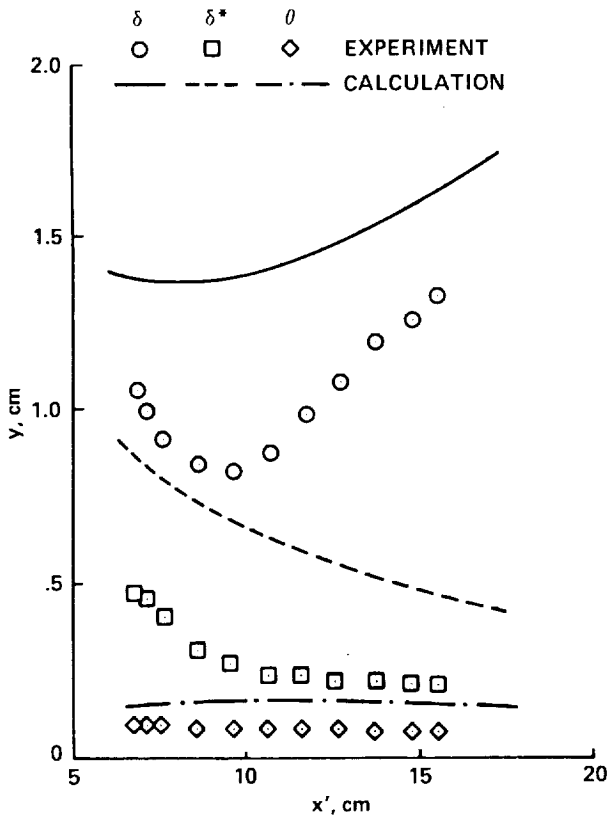


Fig. 9 Comparison of computations and measured boundary-layer thicknesses on the reattachment ramp.

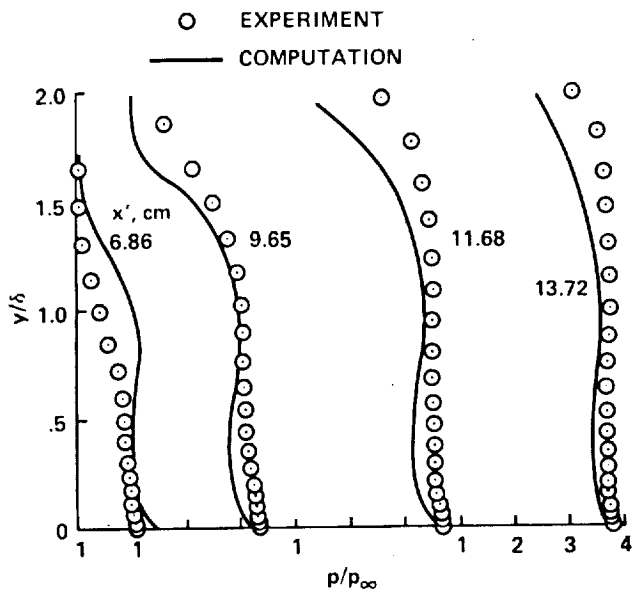


Fig. 10 Comparison of computations and static pressure profile measurements downstream of reattachment.

the choice of δ as a scaling parameter outside the boundary layer.

Figure 11 compares the computed and experimental mean velocity profiles at reattachment and downstream. The computed and measured profiles have similar shapes, but the computation fails to predict

the correct development downstream. The fact that the computed profiles fail to fill out as fast as the measured profiles has also been shown for other experimental test cases downstream of reattachment.^{2,4,15} This deficiency will be discussed in greater detail later. The disagreement between the two profiles at reattachment ($x = 6.86$ cm) is due in part to the fact that the computed solution reattached earlier (at 5.2 cm).

The computed and measured values of the rms mass-flow fluctuations at reattachment and downstream are compared in Fig. 12. Considering the assumptions made to convert the computed kinetic energy to mass-flow fluctuations, the agreement is reasonably good. In the boundary layer the two downstream profiles are well predicted. The profile at reattachment shows the same differences as in the shear layer (Fig. 5). Outside the boundary layer, both the computations and the experiment show the same magnitude of increased fluctuations due to the flow through the recompression shock wave (located near $y/\delta = 1.8$ for the last three stations). However, the vertical extent of this increase is overpredicted. The thickness of the computed recompression shock wave determined from the mean flow quantities was less than 0.15δ (see Fig. 2). At $x = 13.72$ cm the 60% mass-flow fluctuation level outside the boundary layer is calculated from a 12% turbulent kinetic energy level.

At $x = 11.68$ and 13.72 cm the velocity profiles are poorly predicted, but the fluctuation levels are well predicted. Therefore the computed length scale must be in error. Experimental evidence from spark shadowgrams suggests that this portion of the flow field is dominated by large eddies,⁵ which in turn suggests a large increase in turbulence length scale not accounted for in the computed solution.

The computed values of the maximum length scale in the boundary layer, normalized by the local boundary-layer thickness, are shown in Fig. 13. Also shown is the flat-plate value for an equilibrium turbulent boundary layer. These results show a significant increase over the flat-plate value in the reattachment region and downstream, but the previous comparisons with the experiment suggest that this is not enough. To test this hypothesis, the flow field was recomputed while the length scale was increased arbitrarily by a factor of 3 in the middle portion of the boundary layer downstream of reattachment. This resulted in two changes in the computed results: 1) the boundary-layer thickness increased slightly, and 2) the mean velocity profiles changed significantly. A typical profile at $x = 13.72$ cm is shown in Fig. 14. The recomputed velocity distribution with the larger length scale is in much better agreement with the experiment. The kinetic energy distribution remained the same, as is shown in Fig. 12.

These results demonstrate the need for an improved length-scale prediction in the turbulence-model equations. Perhaps the best way to approach this problem is to perform a sensitivity analysis, following Dwyer,¹⁶ to find out which terms or constants in the length scale or dissipation equation need to be modified for improved predictions. This is a formidable task and remains a subject for later study. Also, additional experiments are planned by the Princeton authors of this paper to obtain more direct measurements of the turbulent length scales.

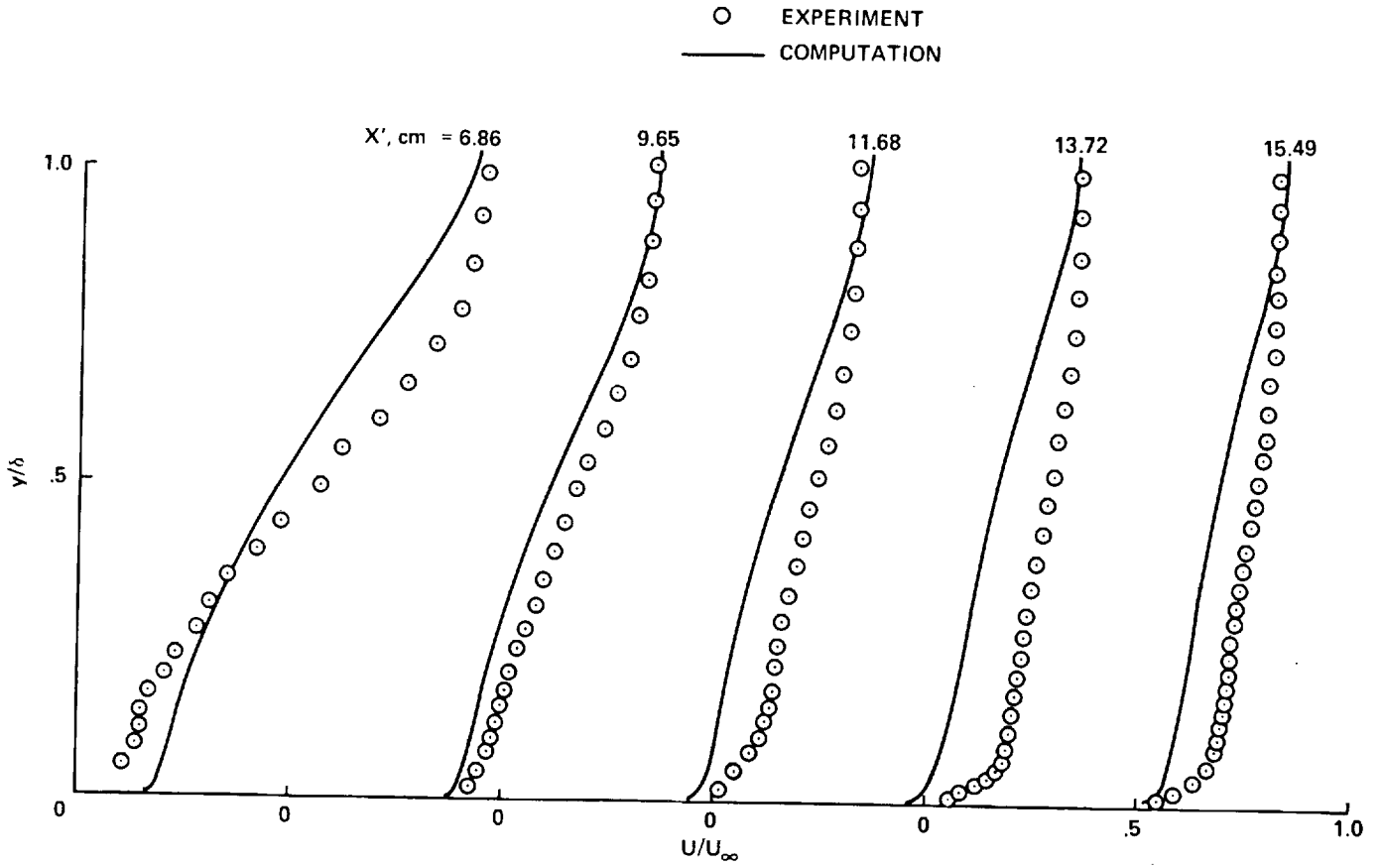


Fig. 11 Comparison of computations and velocity profile measurements downstream of reattachment.

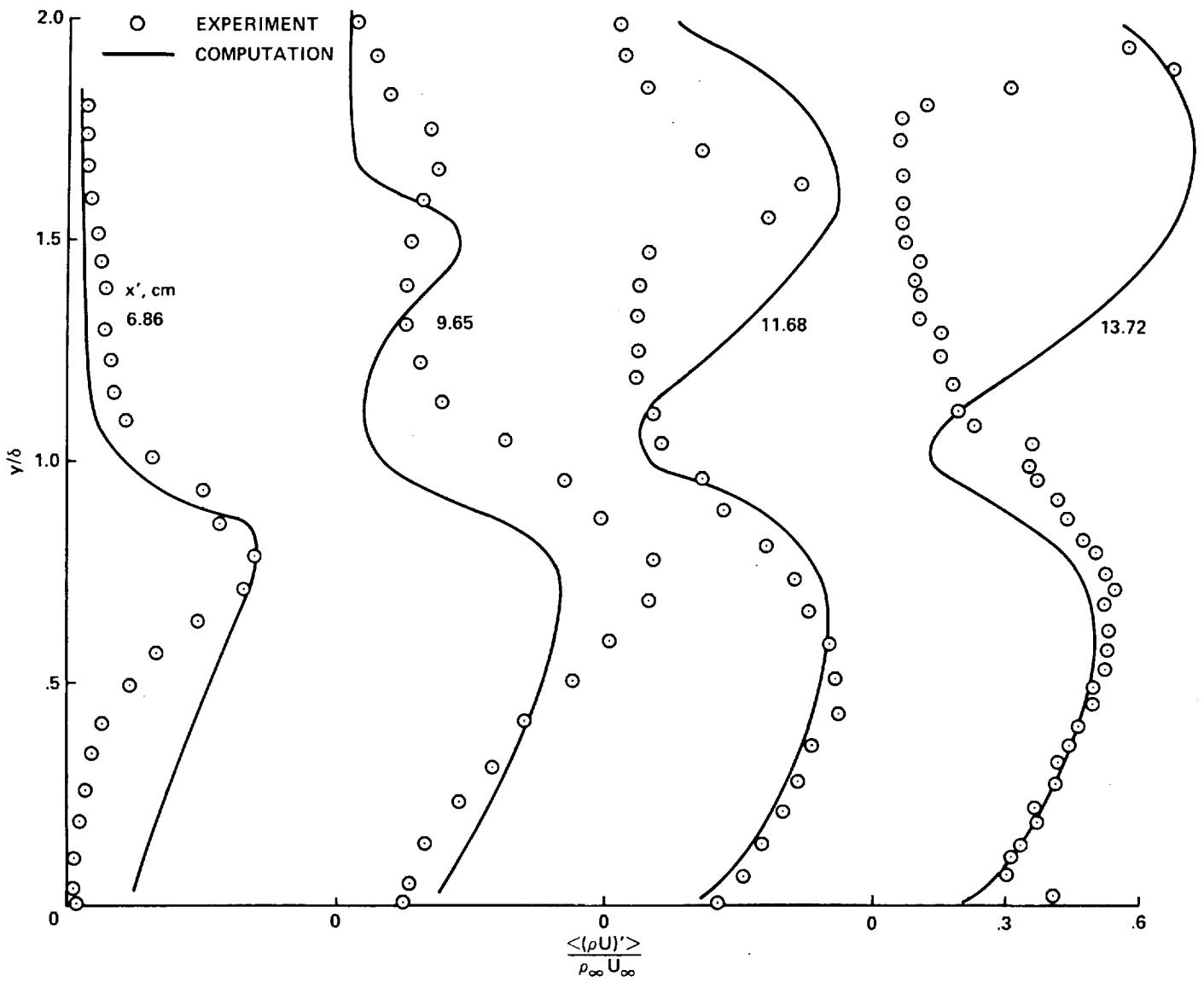


Fig. 12 Comparison of computations and rms mass-flow fluctuation profile measurements downstream of reattachment.

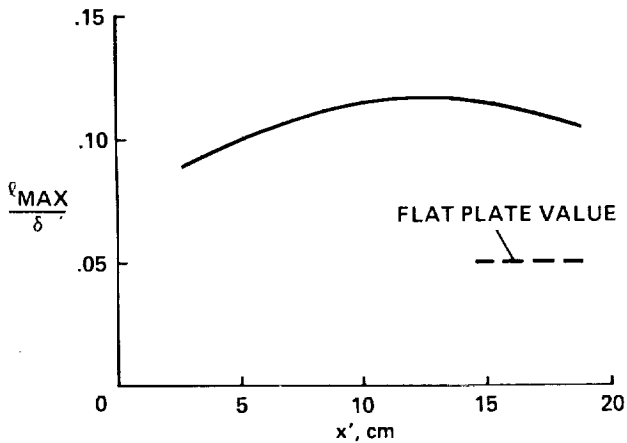


Fig. 13 Computed variation of maximum length-scale downstream of reattachment.

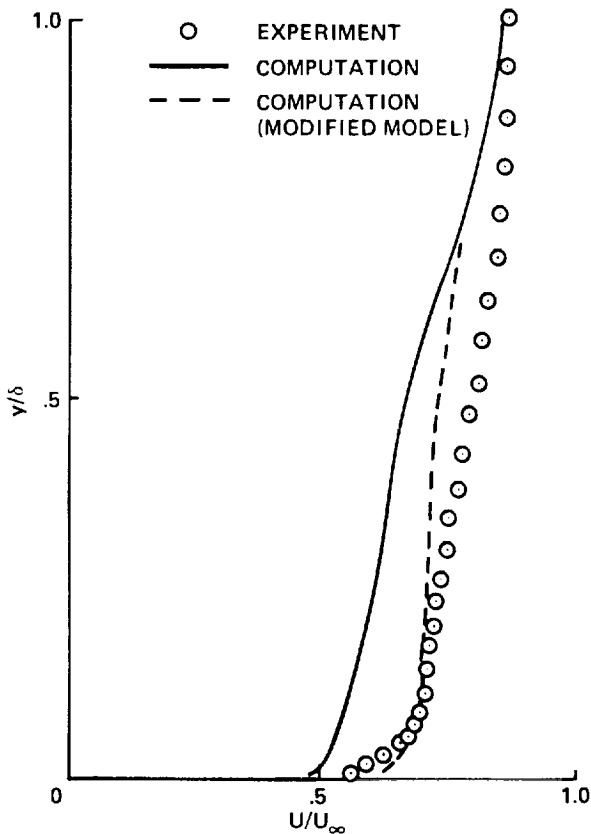


Fig. 14 Comparison of computations with the original and modified turbulence models and velocity profile measurements, $x' = 13.72$ cm.

Conclusions

A detailed experimental documentation of the mean and fluctuating flow throughout a reattaching free shear layer in compressible turbulent flow has been made. These data have been used to assess the validity of corresponding numerical computations and to guide turbulence modeling changes. Numerical solutions of the time-dependent, Reynolds-averaged, Navier-Stokes equations employing a two-equation

turbulence model have been compared with the experimental results. In general, the overall features of this complex flow field have been predicted, although there are several areas of the flow field in which significant improvements in the turbulence modeling are required if good agreement with experiment is to be achieved.

For the free shear layer the numerical results adequately predict the total spreading rate, which is a significant achievement by itself. Also, good agreement was obtained with the detailed velocity profiles in the high-momentum portion of the layer. However, poor agreement was obtained in the low-momentum half of the shear layer, where the mean velocity and the turbulent kinetic energy were over-predicted. This suggests that the turbulence model is producing too much diffusion and that the turbulent length scale is too large in this region.

Because the initial spreading of the computed shear layer into the cavity was too rapid, the computed reattachment point was upstream of the experimental point; as a result, the boundary layer was too thick. Downstream of reattachment, good agreement was obtained with the turbulent mass-flow fluctuations, but the predicted mean velocity profiles failed to develop as rapidly as the experimental ones. This suggested that the computed length scale was underpredicted in this region. An increased length scale was employed in a second computation and improved agreement with the experiment was obtained.

Although the present investigation has not provided an improved turbulence model, it has isolated the area where improvements are needed, namely the second turbulence model equation for the dissipation rate, which determines the length scale. Before such improvements can be made, a sensitivity analysis must be performed. In the flow studied here we have found two major areas of disagreement; in one the length scale should be decreased and in the other it should be increased. Thus, although the need for turbulence model improvements is clear, it is significant that at least some features of the experimental flow field were predicted adequately.

References

- ¹Wilcox, D. C. and Rubesin, M. W., "Progress in Turbulence Modeling for Complex Flow Fields, Including Effects of Compressibility," NASA TP-1517, Apr. 1980.
- ²Viegas, J. R. and Horstman, C. C., "Comparison of Multiequation Turbulence Models for Several Shock Boundary-Layer Interaction Flows," *AIAA Journal*, Vol. 17, Aug. 1979, pp. 811-820.
- ³Seegmiller, H. L., Marvin, J. G., and Levy, L. L., Jr., "Steady and Unsteady Transonic Flows," *AIAA Journal*, Vol. 16, Dec. 1978, pp. 1262-1270.
- ⁴Settles, G. S., Fitzpatrick, T. J., and Bogdonoff, S. M., "Detailed Study of Attached and Separated Compression Corner Flow Fields in High Reynolds Number Supersonic Flow," *AIAA Journal*, Vol. 17, June 1979, pp. 579-585.

⁵Settles, G. S., Baca, B. K., Williams, D. R., and Bogdonoff, S. M., "A Study of Reattachment of a Free Shear Layer in Compressible Turbulent Flow," AIAA Paper 80-1408, Snowmass, Colo., July 1980 (submitted to AIAA Journal).

⁶MacCormack, R. W., "Numerical Solution of the Interaction of a Shock Wave With a Laminar Boundary Layer," Lecture Notes in Physics, Vol. 8, Springer-Verlag, 1971, pp. 151-163.

⁷MacCormack, R. W., "An Efficient Numerical Method for Solving the Time-Dependent Compressible Navier-Stokes Equations at High Reynolds Number," Computing in Applied Mechanics, AMD Vol. 18, The American Society of Mechanical Engineers, 1976.

⁸Coakley, T. J. and Viegas, J. R., "Turbulence Modeling of Shock Separated Boundary-Layer Flows," presented at the Symposium on Turbulent Shear Flows, University Park, Pa., Apr. 18-20, 1977.

⁹Schlichting, H., Boundary Layer Theory, McGraw-Hill, New York, 1955.

¹⁰Birch, S. F. and Eggers, J. M., "A Critical Review of the Experimental Data for Developed Free Turbulent Shear Layers," Paper No. 2, NASA SP-321, July 1972.

¹¹Saffman, P. G., "Development of a Complete Model for the Calculation of Turbulent Shear Flows," presented at the 1976 Duke Turbulence Conference, Durham, N.C., Apr. 1976.

¹²Oh, Y. H. and Bushnell, D. M., "Influence of External Disturbances and Compressibility on Free Turbulent Mixing," Paper No. 10, NASA SP-347, Mar. 1975.

¹³Bradshaw, P., "Compressible Turbulent Shear Layers," Annual Review of Fluid Mechanics, Vol. 9, 1977, pp. 33-54.

¹⁴Horstman, C. C. and Rose, W. C., "Hot-Wire Anemometry in Transonic Flow," AIAA Journal, Vol. 15, Mar. 1977, pp. 395-401.

¹⁵Johnson, D. A. and Horstman, C. C., "A Comprehensive Comparison Between Experiment and Prediction for a Transonic Turbulent Flow," AIAA Paper 80-1407, Snowmass, Colo., July 1980.

¹⁶Dwyer, H. A., "A Study of Turbulent Flow with Sensitivity Analysis," AIAA Paper 80-1397, Snowmass, Colo., July 1980.